A high-spatial resolution soil carbon and nitrogen dataset for the northern permafrost region, based on circumpolar land cover upscaling

Juri Palmtag[1], Jaroslav Obu[2], Peter Kuhry[3,4], Andreas Richter[5], Matthias B. Siewert[6], Niels Weiss[7]; Sebastian Westermann[2] and Gustaf Hugelius[3,4]

[1]Department of Human Geography, Stockholm University, Stockholm, Sweden; [2]University of Oslo, Department of Geosciences, Sem Sælands vei 1, 0316 Oslo, Norway; [3]Department of Physical Geography, Stockholm University, Stockholm, Sweden; [4]Bolin Centre for Climate Research, Stockholm University, Stockholm, Sweden; [5] Centre for Microbiology and Environmental Systems Science, University of Vienna, Vienna; [6]Department of Ecology and Environmental Science, Umeå University, Umeå, 901 87, Sweden; [7]Northwest Territories Geological Survey, Government of the Northwest Territories, Yellowknife NT X1A 1K3, Canada.

Corresponding author: Juri Palmtag (juri.palmtag@humangeo.su.se)

Abstract

Soils in the northern high latitudes are a key component in the global carbon cycle; the northern permafrost region covers 22% of the Northern Hemisphere land surface area and holds almost twice as much carbon as the atmosphere. Permafrost soil organic matter stocks represent an enormous long-term carbon sink which is in risk of switching to a net source in the future. Detailed knowledge about the quantity and the mechanisms controlling organic carbon storage is of utmost importance for our understanding of potential impacts of and feedbacks on climate change. Here we present a geospatial dataset of physical and chemical soil properties calculated from 651 soil pedons encompassing more than 6500 samples from 16 different study areas across the northern permafrost region. The aim of our dataset is to provide a basis to describe spatial patterns in soil properties, including quantifying carbon and nitrogen stocks, turnover times, and soil texture. There is a particular need for spatially distributed datasets of soil properties, including vertical and horizontal distribution patterns, for modelling at local, regional or global scales. This paper presents this dataset, describes in detail soil sampling, laboratory analysis and derived soil geochemical parameters, calculations and data clustering. Moreover, we use this dataset to estimate soil organic carbon and total nitrogen storage estimates in soils in the northern circumpolar permafrost region ($17.9 \times 10^6 \, \mathrm{km}^2$) using the ESA's Climate Change Initiative (CCI) Global Land Cover dataset at 300 m pixel resolution. We estimate organic carbon and total nitrogen stocks on a circumpolar scale (excluding Tibet) for the 0-100 cm and 0-300 cm soil depth to be 380 Pg and 813 Pg for carbon and 21 Pg and 55 Pg for nitrogen, respectively. Our organic carbon estimates agree with previous studies, with most recent estimates of 1000 Pg (– 170 to +186 Pg) to 300 cm depth. Two separate datasets are freely available on the Bolin Centre Database repository. Dataset references and DOIs are presented in the "Data access" section in the end.

1. Introduction

Permafrost soils represent a large part of the terrestrial carbon reservoir and form a significant and climate-sensitive component of the global carbon cycle (Hugelius et al., 2014). High-latitude ecosystems are experiencing rapid climate change causing warming of the soil, thawing of permafrost, and fluvial and coastal erosion (Biskaborn et al., 2019; Fritz et al., 2017). Warming enhances the decomposition of organic matter (OM) by microorganisms, which in turn produces carbon dioxide, methane, and nitrous oxide. The release of these greenhouse gases to the atmosphere would in turn generate further climate change, resulting in a positive feedback on global warming (Turetsky et al., 2020). To better predict the magnitude and effect of environmental changes in the permafrost region, improved data on the properties and quantities of carbon and nitrogen stored in these climate vulnerable soils are needed.

In many cases, a lack of observational data for parameterization or evaluation can limit model development or accurate model projections (Flato, 2011). Soil properties such as OM content, soil texture and soil moisture or their derivatives are commonly used to parametrize, train or validate models (e.g. Oleson et al., 2010). Yet, the representation of northern soil profiles in global datasets remains limited (Köchy et al., 2015; Batjes, 2016), the northern circumpolar permafrost region ($20.6 \times 10^6 \, \mathrm{km}^2$) in which permafrost can occur accounts for 22% of the Northern Hemisphere exposed land area (Obu et al, 2019).

Many previous studies have shown a robust relationship between land cover and soil organic carbon (SOC) distribution, making land cover datasets useful for upscaling estimates from soil profiles to full landscape coverage (e.g. Kuhry et al., 2002; Hugelius, 2012; Palmtag et al., 2015; Siewert et al., 2015; Wojcik et al., 2019). Here we describe the compilation of a harmonized soil dataset for permafrost-affected landscapes derived from 15 different high latitude sites and one high alpine study site in Canada, Greenland, Svalbard, Sweden, and Russia (Fig. 1; Table 1). In total, 651 soil pedons contain information from up to 6529 samples on carbon and nitrogen content, carbon to nitrogen (C/N) ratio, isotopic composition, texture (sand, silt + clay) and coarse fraction content, land cover type, wet and dry bulk density, calculated volumetric contents for ice/water, and volumetric content of organic soil material, mineral soil material and air. ~~In addition, soil pedon descriptions include metadata on actual sampling site, coordinates and elevation, slope and aspect, drainage, percentage of stones and boulders, landform, and maximum sampling depth.~~ Site data were upscaled to the northern circumpolar permafrost region using the European Space Agency (ESA) Climate Change Initiative (CCI) Global Land Cover dataset at 300 m pixel resolution, which is the very first long-term global land cover time series product.

This study has two main aims. Firstly, the ~~core~~ primary ~~objective~~ aim of this dataset is to provide a harmonized, high resolution, quality controlled, and contextualized soil pedon dataset with a focus on SOC, nitrogen and other parameters essential to determine the role of northern permafrost region soils in the climate system. Particularly, the extensive metadata on soil properties included for many samples when available (texture, volumetric densities, active layer depth, ice content, isotopic composition, etc.) are of great importance and can be used to identify and model the processes responsible for the current and future carbon balance. Secondly, ~~to~~ we used th~~is~~e soil dataset and an existing spatial product for upscaling to provide a new and independent estimate of the ~~soil organic carbon~~SOC and total nitrogen (TN) storage estimates within the northern circumpolar permafrost region. ~~Particularly, the extensive metadata on soil properties included for many samples when available (texture, volumetric densities, active layer depth, ice content, isotopic composition, etc.) are of great importance and can be used to identify and model the processes responsible for the current and future carbon balance.~~
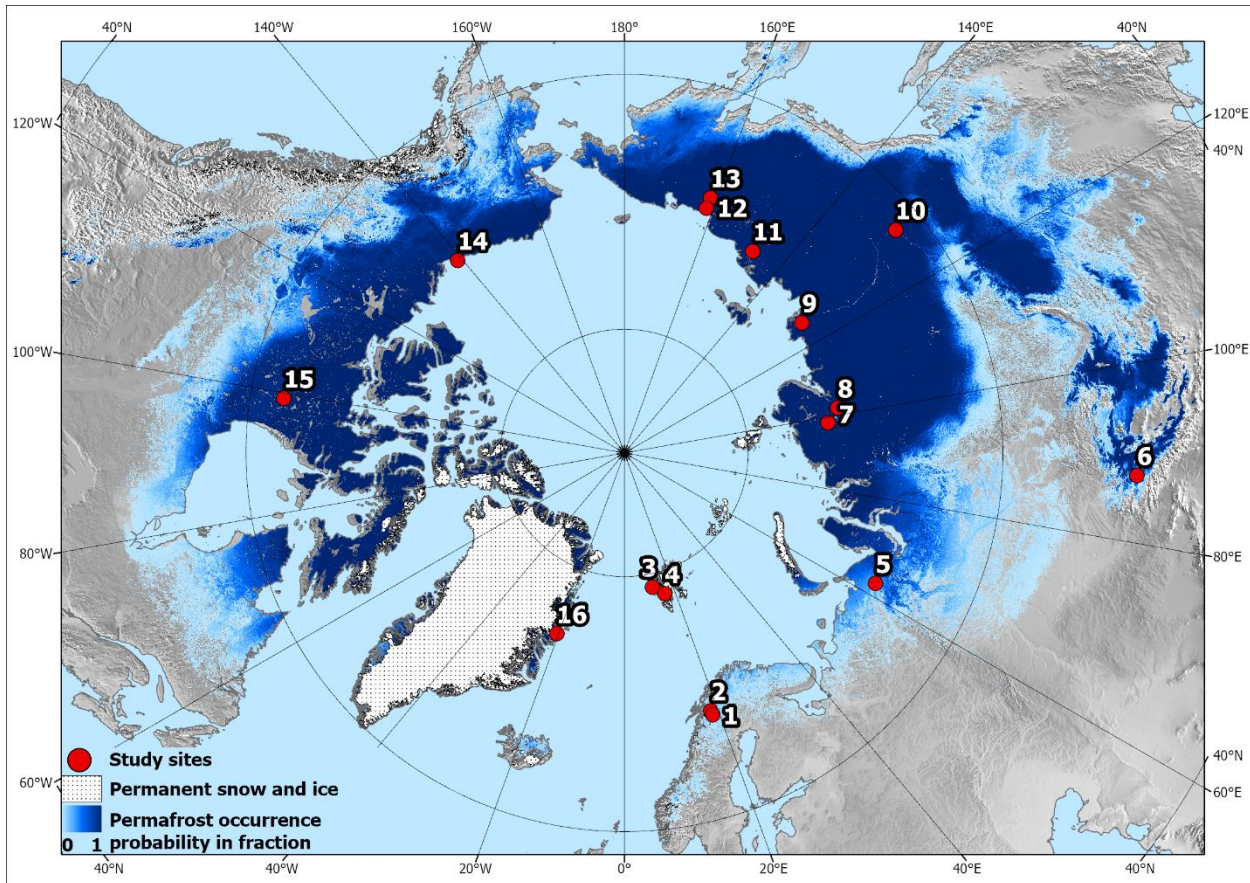
Figure 1: Overview map with location of the 16 sampling sites (see Table 1). Blue shading indicates permafrost probability (dark hues showing higher permafrost occurrence probability), based on an equilibrium state model for the temperature at the top of the permafrost (TTOP) for the 2000–2016 period (Obu et al., 2019). North Pole Lambert azimuthal equal area projection (datum: WGS 84). Base map: Made with Natural Earth.

2.Methods

2.1 Dataset structure

The dataset contains 6529 analyzed samples from 651 soil pedons in 16 different sampling locations across the northern permafrost region (Fig 1; Table 1) (Palmtag et al., 2022a, b). Each sampled pedon was described and classified according to land cover type. Land cover is defined as the biophysical cover of the Earth's terrestrial surface such as different vegetation types, water, and bare ground.

94   Table 1: Summary of all study sites

Nr.	Study area	Country	Long	Lat	n=pedons	Reference
1	Tarfala	Sweden	18.63° E	67.91° N	55	Fuchs et al., 2015
2	Abisko	Sweden	18.05° E	68.33° N	125	Siewert, 2018
3	Ny Ålesund	Norway	11.83° E	78.93° N	28	Wojcik et al., 2019
4	Adventdalen	Norway	16.04° E	78.17° N	48	Weiss et al., 2017
5	Seida, Usa River Basin	Russia	62.55° E	67.35° N	44	Hugelius et al., 2009; 2011
6	Aktru, Altai mountains	Russia	87.47° E	50.05° N	39	Pascual et al., 2020
7	Logata, Taymyr	Russia	98.42° E	73.43° N	31	Palmtag et al., 2016
8	Arymas, Taymyr	Russia	101.90° E	72.47° N	35	Palmtag et al., 2016
9	Lena Delta	Russia	126.22° E	72.28° N	56	Siewert et al., 2016
10	Spasskaya Pad	Russia	129.46° E	62.25° N	33	Siewert et al., 2015
11	Tjokurdach	Russia	147.48° E	70.83° N	27	Siewert et al., 2015; Weiss et al., 2016
12	Shalaurovo	Russia	161.55° E	69.32° N	22	Palmtag et al., 2015
13	Cherskiy	Russia	161.30° E	68.45° N	15	Palmtag et al., 2015
14	Herschel Island	Canada	139.09° W	69.58° N	42	Siewert et al., 2021
15	Tulemalu Lake	Canada	99.16° W	62.55° N	16	Hugelius et al., 2010
16	Zackenberg	Greenland	20.50° W	74.45° N	35	Palmtag et al., 2015; 2018

95

96   Land cover products are commonly satellite derived and sometimes globally available. We opted for a two-tier
97   approach, where more classes can be used in products with higher thematic or spatial resolution (Table 2). First, we
98   differentiated land cover into 5 primary tier classes (Tier I) which represent the major land cover types: forest, tundra,
99   wetland, barren, and Yedoma. Although Yedoma is a sedimentary deposit and not a typical land cover class, it was
100   added due to its large areal extent, special soil organic matter (SOM) and ground ice properties, as well as soil
101   characteristics (Strauss et al., 2017; Weiss et al., 2016). Subsequently, Tier I classes were subdivided into 10 Tier II
102   subclasses (Table 2).

103

104 Table 2: Hierarchical structure of the two-tier land cover class system applied to the pedons based on field
105 observations.

TIER I		TIER II	
1	Forest	1.1	Deciduous broadleaf forest
		1.2	Evergreen needleleaf forest
		1.3	Deciduous needleleaf forest
2	Tundra	2.1	Shrub tundra
		2.2	Graminoid / forb tundra
3	Wetland	3.1	Permafrost wetlands
		3.2	Non-permafrost wetlands
4	Barren	4.1	Barren
5	Yedoma	5.1	Yedoma tundra
		5.2	Yedoma forest

106 **2.1.1 Class definitions of soil pedons to land cover types**

107 All sampling sites were classified with Tier I descriptions using field descriptions and, where possible, assigned a
108 more detailed (Tier II) description. The forest class was used for sparse to dense forests, further separated into three
109 different Tier II classes: deciduous broadleaf, evergreen needleleaf and deciduous needleleaf forest. Tundra is
110 separated in Tier II to shrub tundra (dominated by erect shrubs > 50 cm height) and graminoid / forb tundra (with low
111 growth heath vegetation or graminoid dominated). Wetland includes terrain that is saturated with water for sufficient
112 time of the year to promote aquatic soil processes with low oxygen conditions and occurrence of vegetation fully
113 adapted to these conditions, as well as all types of peatlands. Areas that met the National Wetlands Working Group
114 (1997) definition of a wetland were classified as such. We applied a classification that is adapted from the Canadian
115 system (National Wetlands Working Group, 1997) describing the wetlands in the field and following types of wetlands
116 were included to the Tier I wetland class: organic, mineral, seasonal, permanent, ombrotrophic and minerotrophic
117 wetlands. The permafrost status within the top 2 m of a site was used to distinguish in Tier II the permafrost wetlands
118 and the non-permafrost wetlands. Although a substantial part of the northern circumpolar permafrost region is
119 classified as water ($0.98 \times 10^6 \, \text{km}^2$) or permanent snow/ice ($0.06 \times 10^6 \, \text{km}^2$), no soil sample or pedon data from these
120 classes are included in the database. The Tibetan permafrost region was also excluded from our estimates as none of
121 the sampling sites originated from that area. The class barren includes land cover types such as exposed bedrock,
122 boulder fields, talus slopes, debris cones, rock glaciers, where soil is either almost completely absent, or occurs only
123 in minor patches (<10 % area) or in between boulders. The land cover class Yedoma is defined as areas in Siberia,
124 Alaska, and Yukon underlain by late Pleistocene ice-rich syngenetic permafrost deposits. We used the spatial extent

125 for the Yedoma domain from Strauss et al. (2017) which occupied an area of 570,000 km^2 from ~~here~~ the used ESA

126 CCI land cover product. Tier II divides the Yedoma domain into Yedoma tundra and Yedoma forest.

2.2 Soil sampling

128 Field soil sampling took place in summer months (late June to early September) between 2006 and 2019, most

129 frequently in August or September in order to capture the maximum seasonal thaw (active layer) depth at each site.

130 Active layer thickness was measured at each location using a graduated steel probe or measuring tape in excavated

131 soil pits. A stratified sampling scheme ~~(582 out of 651)~~ consisting of linear transects with predefined equidistant

132 intervals of typically 100 to 200 m across all major landscape elements was used to retrieve soil pedons (n = 582),

133 with on average 37 sampling sites per study area. To ensure that this sampling scheme covered all representative

134 landscape units and types, maps (including vegetation, surficial geology) and remote sensing products (including air

135 photos, satellite imagery, and elevation models) were assessed prior to fieldwork. Detailed field reconnaissance

136 involving visual observation of the manageable study area were conducted before establishing transects. Sampling

137 sites were located and marked at the exact position based on distance to the first sampling point and compass bearing

138 using a hand-held GPS device. This ensured an unbiased location of individual sampling sites. When sufficient time

139 was available in the field, additional sampling (n = 69) using a random or stratified random distribution of sampling

140 points was used. Following the field sampling protocol (Figure S1), a site description, soil and in several cases

141 phytomass sampling were conducted at each sampling point.

142 For each pedon, the organic layer ~~(OL)~~ and the active layer was sampled from an open soil pit excavated to the bottom

143 of the active layer, to the bedrock or when this was not possible, to a depth of at least 50 cm~~to at least reach a depth~~

144 ~~beyond ± 50 cm~~ (Fig. 2). Deeper unfrozen soil layers were sampled using a steel pipe (see permafrost sampling below).

145 The organic layer sample was cut out as a block using a pair of scissors or a knife (removing living vegetation), and

146 the block volume was measured in the field. The active layer samples were collected using 100 cm^3 soil sampling

147 rings inserted horizontally into the soil profile. Sampling of the active layer was performed in fixed depth intervals

148 (5–10 cm) or along soil horizon boundaries. For non-permafrost wetland sites, a Russian peat corer with a 50 cm long

149 chamber was used. After extraction, the core was ~~described and~~ subdivided into smaller increments (generally 5 cm)

150 which~~. This~~ resulted typically in about 5–15 samples per sampling site depending on the reached depth.

151 The permafrost section of the soil profile and very deep unfrozen soil layers were sampled using a steel pipe that was

152 hammered into the ground in short (5 to 10 cm) depth increments. The pipe was pulled out after each sampled

153 increment using large pipe wrenches, and the sample was pushed out of the pipe using a steel rod. At several locations

154 (n = 18) permafrost samples were also collected from exposures along lake shores or river valleys where the steel pipe

155 was hammered in horizontally. These steel pipes are industry standardized with an outer diameter of 42.2 mm (1.25

156 inches), affordable and widely available even in remote locations. At several locations (n = 5), soil cores were collected

157 using a handheld motorized rotational Earth Auger (Stihl BT 121) with a 50 cm core barrel and 52 mm outside

158 diameter. Samples were split lengthwise into two halves: one half was analyzed to determine sediment characteristics,

159 volumetric ice content, and gravimetric water content. Disturbance material was removed from the core surface by
160 repeated scraping with a razor blade. ~~All half-cores were then photographed and described in detail.~~ The other half of
161 each core was kept as a frozen archive to be used in the event of laboratory error. Since the accurate determination of
162 soil bulk density (BD) is crucial when calculating SOC~~converting sample weight to volume or area and is essential to~~
163 ~~calculate SOC stocks. Therefore~~, special attention was paid to accurate soil volume estimation during field sampling.
164 The target depth for soil cores was 100 cm, or until bedrock or massive ground ice (e.g. ice-wedges) was reached.
165 Pedons were often extended beyond 100 cm depth (n = 313), in particular to assess full peat depth and organic/mineral
166 transition in organic soils.

167 ~~All samples were described in the field and packed into sampling bags.~~ Wet or frozen samples were described and
168 placed in double bags to assure no soil water was lost in transport. For each sampled soil profile, pictures and notes
169 were taken to describe land cover type, landform, elevation, slope and aspect, surface moisture, and surface features.
170 Specific observations regarding the collected sample depths, such as excess ground ice (visual estimate, %),
171 occurrence of large stones (visual estimate, %), colour (general description or using a Munsell scale), soil structure,
172 including signs of cryoturbation, roots and rooting depth were noted. Samples with cryoturbated soil material were
173 marked or rated on a scale from 1 to 3 according to the relative amount of cryoturbated soil material. Soil texture,
174 which refers to particle size and relative content of mineral components (sand, silt + clay) is of importance as it affects
175 the physical and chemical properties of a soil, including cryoturbation (Palmtag and Kuhry, 2018). Soil texture was
176 estimated for most samples using manipulation tests and assessment by hand in the field under varying weather
177 conditions. To avoid misinterpretation, we decided to combine silt and clay and refer to them as one fine-grained soil
178 texture class. In case of permafrost samples, subsamples were thawed, analyzed and returned back to the sample bag.
179 ~~To avoid misinterpretation, we decided to combine silt and clay and refer to them as one fine-grained soil texture~~
180 ~~class.~~ The land cover and vegetation community were described at all sites. For many sites, vegetation cover was
181 described in terms of relative plant functional type coverage per square meter. Beyond assigning the profiles to land
182 cover, vegetation data is not included in this database and not further discussed.

183

184
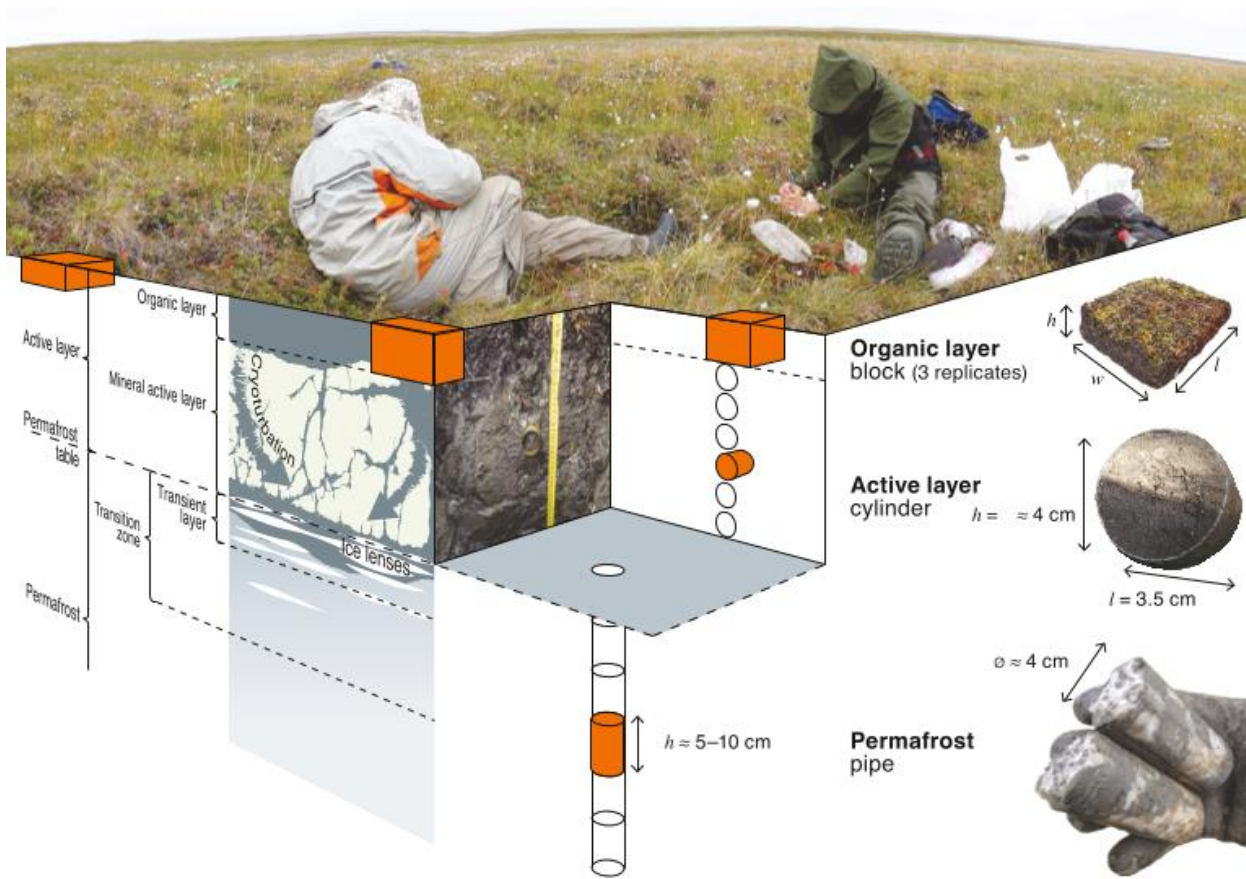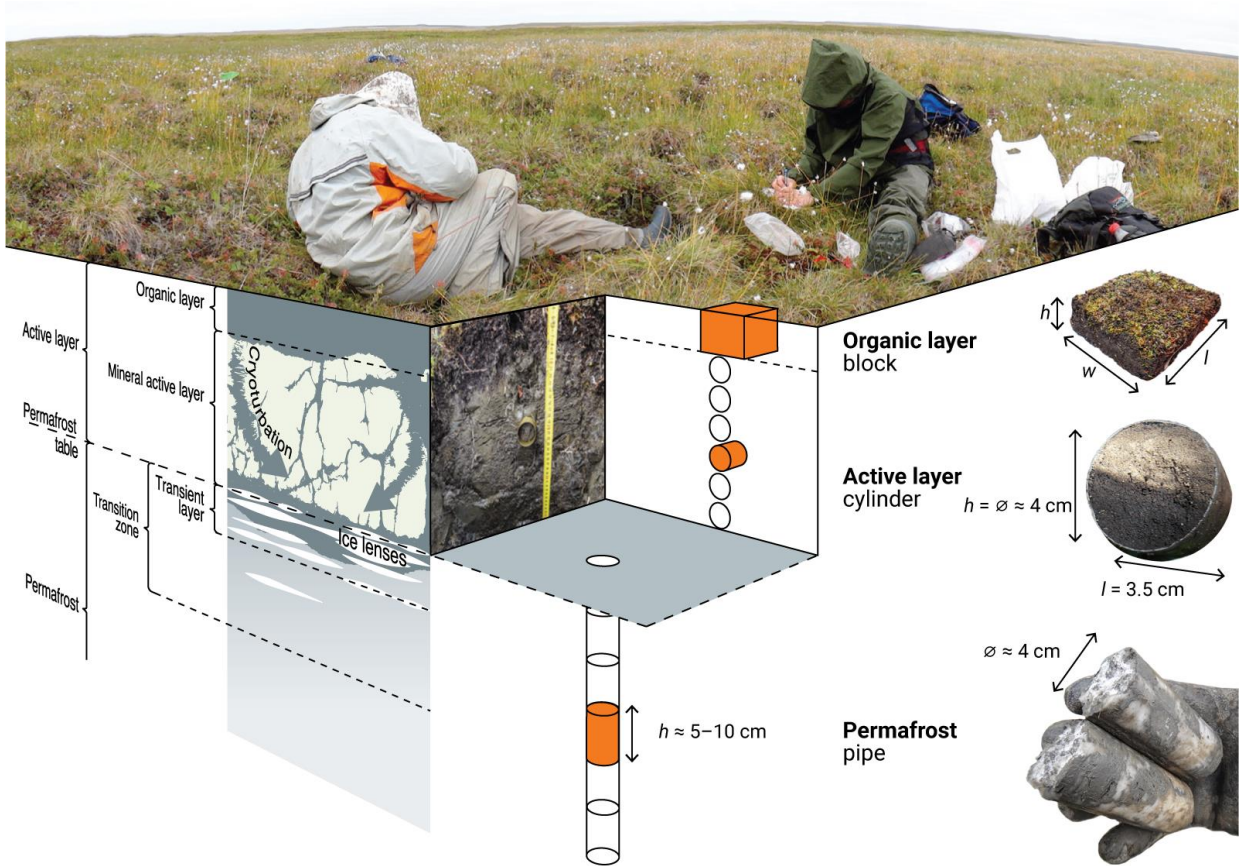
Figure 2: A three-dimensional field sampling protocol with typical soil layers in permafrost ground (reprinted from Weiss 2017, p.12). The orange shapes represent the different sampling techniques for organic surface layer (block), active layer sample from an excavated pit (fixed volume cylinder) and permafrost sampling (steel pipe).

2.3 Laboratory analysis

In the laboratory, soil samples (n = 5315) were weighed before and after oven-drying at 60-70° C for at least 24 h (or until no further weight change was observed) to determine field-moist mass (m_{ws}) and the oven-dried mass (m_d), thus permitting the calculation of wet bulk density (BD_w) and dry bulk density (BD, g cm^{-3}) using the known sample volume. To ensure that there was no remaining water in the organic rich and/or fine grained samples (n=3684), subsamples of ~10 g were dried again at 105 C to verify the oven dried weights. ~~From organic rich and fine grained samples (n = 3684), subsamples of around 10 g were dried again at 105° C to verify dry weight and correct in case not all water was lost at the lower temperature. Remaining samples which were not dried again, were sand or course grain samples and showed in tests no noteworthy differences. The reason for the main sample being dried at lower temperature is to ensure that samples can be dried in the original plastic sample bags (without loss of sampled materials) and subsequently used for additional analyses that may be sensitive to the higher drying temperature (results from such additional analyses are not included here).~~ After drying, samples were homogenized and sieved to determine

200 the concentration of coarse mineral fragments (CF, >2 mm, %). For a subset of samples, particle size analysis was
201 performed using a Malvern Mastersizer 3000 laser particle size analyzer (Malvern Instruments Ltd, Malvern, UK),
202 which can analyze particles in the range of 0.01–3500 μm in diameter. It measures the intensity of light scattered as a
203 laser beam passes through a dispersed particulate sample. A detailed description of these samples is given in Palmtag
204 et al. (2018). Out of 5331 samples where OC % data is available, subsamples from 4471 samples were ~~burned~~ heated
205 to 550° C for 5h ~~at 550° C~~ to obtain organic matter content through loss on ignition (LOI; Heiri et al., 2001), and about
206 half of the samples (n = 2960), were ~~burned at~~ heated to 950° C for 2 h to determine carbonate content (for details, see
207 Palmtag et al., 2015; 2016). To determine the elemental content of carbon and nitrogen (TOC and TN) and their
208 isotopic composition, 2674 samples were analysed using an Elemental Analyser (EA). If LOI950 following Heiri et
209 al. (2001) indicated presence of inorganic carbon ~~with~~ > 1%, samples were acid treated (Abisko, Sweden; Ny Ålesund,
210 Norway; Aktru, Altai mountains, Russia) with hydrochloric acid prior to determination of TOC. To estimate the
211 organic carbon % (OC %) for samples where only LOI was available (44 %), a polynomial regression model (R^2 =
212 95%) was performed between LOI550 and OC % from EA on samples for which both analyses were available at study
213 area level.

214 ~~Carbon to nitrogen ratios are often used as an indicator for SOM decomposition. As during the metabolic activity by~~
215 ~~microorganisms more carbon than nitrogen is released, the C/N ratio decreases with a higher degree of humification.~~
216 ~~This is why C/N ratios usually decrease with depth, as deeper layers are typically older and more decomposed (Kuhry~~
217 ~~and Vitt, 1996). The C/N ratios together with stable carbon isotopes (δ^{13}C) can be used to gain insight into the~~
218 ~~biochemical processes of SOM, botanical origin with depth and the degradation state (Kracht and Gleixner, 2000).~~

219 **2.4 SOC/TN stock calculations and upscaling**

220 Dry and wet bulk density (g cm^{-3}), sample volume (cm^3) and % carbon was used to calculate the volumetric contents
221 of water, organic soil material, mineral soil material and air for each sample. The soil organic carbon content (kg C
222 m^{-2}) was calculated for each sample separately based on dry bulk density (BD, g cm^{-3}), percentage organic C in the
223 sample (OC %), sample thickness T (cm), and coarse fraction correction (CF) (Equation 1). Equation 1 was also used
224 to calculate the TN content, in which OC % was replaced with N %.

225 $$SOC(gC\,cm^{-2}) = BD * OC\,\% * (1 - CF) * T \hspace{4cm} 1$$

226 SOC content for each pedon was calculated by summing up individual samples on 1 cm resolution until the maximum
227 sampling depth was reached. The pedons were assigned to a specific land cover class and the SOC content averaged
228 for different depth intervals (0–30 cm, 30–50 cm, 50–100 cm, 100–200 cm, 200–300 cm, and summed to 0–100 cm
229 and 0–300 cm). In areas with large stones in the soil column (e.g. alpine areas) or areas with massive ice bodies (e.g.
230 Yedoma deposits), it is also important to deduct the volume of stones or massive ice from the calculations. These
231 additional variables are not included in equation 1, but were accounted for in the SOC calculations at the pedon level.
232 If bedrock was encountered at any point, a SOC content of 0 kg C m^{-2} was assigned for the remaining part down to
233 300 cm depth at that specific sampling site. In pedons where some increments were missing or the full sampling depth

234 was not reached, the nearest samples from the same pedon for BD and OC % were interpolated or extrapolated. To

235 avoid overestimation of the SOC storage, such extrapolations were only used where field notes showed that the

236 deposits were homogeneous and bedrock was not reached.

237 Masses of soil components (water (m_w, g), organic matter (m_{OM}, g) and mineral component (m_{min}, g)) were calculated

238 based on the laboratory analysis for all the individual samples. The mass of water was calculated as a difference

239 between field-moist mass and oven-dried mass. Organic matter mass was calculated from the OC % and dry sample

240 weight and multiplied by 2, which is a standard conversion factor between SOC and SOM (Pribyl, 2010). The mass

241 of the mineral fraction was calculated as a difference between dry sample mass and organic matter mass.

242 Volumetric fractions of soil components were calculated by dividing the volume of the component with the total

243 sample volume (V). We calculated component volumes from mass by assuming the following densities: 1 g cm^{-3} for

244 water, 0.91 g cm^{-3} for ice, 1.3 g cm^{-3} for organic matter (Farouki, 1981) and 2.65 g cm^{-3} mineral component. The

245 volumetric fraction of air was calculated as one minus the sum of the other fractions.

246 All profiles were assigned to land cover class based on field descriptions. Dry bulk density, SOC density, TN density

247 and the volumetric contents of mineral and organic matter and water and air were averaged according to land cover

248 classes for depths until 3 m using Python scripting language and pandas library (McKinney, 2011). Soil parameters

249 were assigned to pedon sample depth ranges and these were grouped according to land cover classes yielding means

250 and standard deviations for each centimetre of depth. Fractions of soil texture classes (sand and silt + clay) were

251 created using the same procedure by counting occurrences of texture classes within pedons. Typical soil stratigraphies

252 were generated for each class which can be used as input for permafrost modelling and mapping (e.g. Westermann et

253 al., 2013; 2017; Czekirda et al., 2019).

254 For the upscaling, we used the land cover map from the Global ESA Land cover Climate Change Initiative (CCI)

255 project at 300 m spatial resolution (http://maps.elie.ucl.ac.be/CCI/viewer/index.php). The overall classification

256 accuracy, based on 3167 random sampling cases, is stated as 73 % (Defourny et al., 2008). The land cover class dataset

257 for upscaling was generated from ESA CCI land cover yearly products from period 2006 to 2015 (corresponding to

258 the sampling period) by identifying prevailing land cover classes within this period. The extent of the Yedoma land

259 cover classes was defined from shapefiles of the Yedoma database by Strauss et al., (2017), where all the layers were

260 used except for QG2500k, which is showing the lowest probability of Yedoma occurrence.

261 Since the ESA land cover product uses a different nomenclature for land cover types with different sub-categories,

262 similar classes were amalgamated to fit our tiered land cover system (Table 2). Several minor classes consisting of

263 single pixels spread over the map were generalized and merged with the class surrounding the pixel. We defined Tier

264 II Yedoma classes (Yedoma tundra and Yedoma forest) according to the ESA CCI Land cover classes coinciding with

265 Yedoma deposits (Table 3).

266 The spatial land cover extent was constrained to the Northern Hemisphere permafrost region indicating probability of

267 permafrost occurrence but not the actual area underlain by permafrost (Obu, 2021). This dataset stretches over

268   17.9×10^6 km^2 of the Northern Hemisphere, and is based on equilibrium state model for the temperature at the top of

269   the permafrost (TTOP) for the 2000–2016 period (Obu et al., 2019).

270   Table 3: Amalgamation of ESA's CCI land cover classes with the Tier class system above the Yedoma deposits.

CCI class	ESA CCI landcover	TIER I class	TIER II class
40	Mosaic natural vegetation (tree, shrub, herbaceous cover) (>50 %)	1	1.1 & 5.2
50	Tree cover, broadleaved, evergreen, closed to open (>15 %)	1	1.1 & 5.2
60	Tree cover, broadleaved, deciduous, closed to open (>15 %)	1	1.1 & 5.2
61	Tree cover, broadleaved, deciduous, closed (>40 %)	1	1.1 & 5.2
70	Tree cover, needleleaved, evergreen, closed to open (>15 %)	1	1.2 & 5.2
71	Tree cover, needleleaved, evergreen, closed (>40 %)	1	1.2 & 5.2
72	Tree cover, needleleaved, evergreen, open (15-40 %)	1	1.2 & 5.2
80	Tree cover, needleleaved, deciduous, closed to open (>15 %)	1	1.3 & 5.2
90	Tree cover, mixed leaf type (broadleaved and needleleaved)	1	1.1 & 5.2
100	Mosaic tree and shrub (>50 %) / herbaceous cover (<50 %)	1	1.1 & 5.2
110	Mosaic herbaceous cover (>50 %) / tree and shrub (<50 %)	1	1.3 & 5.2
120	Shrubland	2	2.1 & 5.1
121	Evergreen shrubland	2	2.1 & 5.1
122	Deciduous shrubland	2	2.1 & 5.1
130	Grassland	2	2.2 & 5.1
140	Lichens and mosses	2	2.2 & 5.1
150	Sparse vegetation (tree, shrub, herbaceous cover) (<15 %)	2	2.1 & 5.1
152	Sparse shrub (<15 %)	2	2.1 & 5.1
160	Tree cover, flooded, fresh or brackish water	3	3.1
180	Shrub or herbaceous cover, flooded, fresh/saline/brackish water	3	3.1
200	Bare areas	5	4.1
201	Consolidated bare areas	5	4.1
202	Unconsolidated bare areas	5	4.1

271

272   The upscaling to estimate the total carbon storage in the northern circumpolar permafrost region was performed in

273   ArcGIS Pro (ESRI, Redlands, CA, USA) by multiplying the mean SOC storage for each ~~tier~~ Tier I and ~~tier~~ Tier II

274   class with the spatial extent of the corresponding CCI land cover class. To determine reasonable error estimates for

275   carbon stocks within the permafrost region, we used a spatially weighed 95 % confidence interval (CI) as described

276   by Thompson (1992) assuming that our residuals are normally distributed (Hugelius, 2012).

277     $$CI = t * \sqrt{\Sigma\left(\left(a_i^2 * SD_i^2\right)/n_i\right)} \qquad\qquad 2$$

278   The CI accounts for the relative spatial extent, carbon stock variations in pedons and number of replicates in each

279   upscaling class. Replicates were only considered for pedons reaching the full sampling depth, resulting in fewer

280 replicates available with increasing sampling depth. In equation 2: *t* is the upper α/2 of a normal distribution (t ≈ 1.96),

281 *a* the % of the area; *SD* is the standard deviation, *n* is to the number of replicates and *i* refers the specific Tier class.

3. Results

3.1 SOC estimates

284 Using our pedon based dataset, we obtain SOC stock estimates within the northern circumpolar permafrost region of

285 379.7 and 812.6 Pg for 0–100 cm and 0–300 cm depth, respectively. Table 4 shows mean SOC storage (kg C m^{-2}) and

286 total SOC stock for all depth increments, including 95 % confidence intervals. The upscaling using this new pedon

287 data shows that almost half of SOC in the northern circumpolar permafrost region is stored in the top meter. The three

288 most abundant classes together (deciduous needleleaf forest, shrub tundra and graminoid / forb tundra) occupy 67 %

289 of the permafrost region (Table 5) and store most of terrestrial SOC in the northern circumpolar region (74 %). The

290 permafrost wetland class has the largest SOC content to 300 cm with 112.2 kg C m^{-2}, but has only a small areal

291 coverage in the ESA LCC product (1.4 %) which results in a total SOC storage contribution of 3.5 % within the

292 permafrost region. Figure 3 illustrates the spatial distribution of total SOC storage (kg C m^{-2}) to a depth of 0–100 cm

293 and 0–300 cm for the circumpolar permafrost region. Spatially, the SOC distribution in Figure 3 is following the same

294 pattern and ~~is~~ highlight~~sing~~ the largest SOC content predominantly in ~~mostly~~ permafrost peatlands in Western Siberia,

295 Russia and the Nunavut territory in Canada. Despite that, more than 77% of the area has a SOC storage to a depth of

296 300 cm higher than 50 kg m^{-2}.

297 Table 4: Landscape mean and total SOC storage with 95 % CI for the different depth increments for the northern
298 circumpolar permafrost region, excluding water bodies and permanent snow and ice.

Depth increment	n:	~~Landscape mean~~ Mean SOC storage (kg C m^{-2})	95 % CI [a]		Total SOC in Pg	95 % CI [a]	
0–30 cm	452	9.0	±	1.4	160.0	±	25
30–50 cm	402	3.9	±	0.5	69.2	±	8
50–100 cm	328	8.4	±	1.4	150.5	±	25
100–200 cm	257	12.4	±	1.9	222.0	±	35
200–300 cm	253	11.8	±	1.7	211.0	±	31
0–100 cm	328	21.3	±	3.2	379.7	±	58
0–300 cm	253	45.5	±	7.6	812.6	±	136

299

300 [a] The 95 % confidence interval refers to landscape mean SOC storage and total SOC storage

Table 5: Mean and total SOC storage for (A) 0–100 cm and (B) 0–300 cm soil depth separated for the different Tier classes in the northern circumpolar permafrost region, excluding water bodies and permanent snow and ice.

A	Tier class	LCC class	n [a]:	Area (million km^2)	Area %	Mean SOC storage (kg C m^{-2}) [b]	SD [b]	Total SOC in Pg	Total SOC storage %
	1.1	Deciduous broadleaf forest	5	0.85	4.8 %	16.5	9.3	14.1	3.7
	1.2	Evergreen needleleaf forest	4	2.54	14.3 %	14.6	12.8	37.1	9.8
	1.3	Deciduous needleleaf forest	28	5.20	29.1 %	20.5	20.3	106.5	28.1
	2.1	Shrub tundra	54	3.97	22.3 %	22.3	21.7	88.5	23.3
	2.2	Graminoid / forb tundra	118	2.85	15.9 %	31.6	23.0	90.0	23.7
	3.1	Permafrost wetlands	61	0.25	1.4 %	37.8	37.8	9.6	2.5
	3.2	Non-permafrost wetlands	10	0.76	4.3 %	17.8	14.7	13.5	3.6
	5.1	Barren	39	0.85	4.8 %	9.4	12.0	8.0	2.1
	7.1	Yedoma tundra	8	0.27	1.5 %	28.1	17.0	7.7	2.0
	7.2	Yedoma forest	1	0.30	1.7 %	16.1	0.0	4.8	1.3

B	Tier class	LCC class	n [a]:	Area (million km^2)	Area %	Mean SOC storage (kg C m^{-2}) [b]	SD [b]	Total SOC in Pg	Total SOC storage %
	1.1	Deciduous broadleaf forest	2	0.85	4.8 %	33.2	22.8	28.3	3.5
	1.2	Evergreen needleleaf forest	2	2.54	14.3 %	23.0	16.3	58.7	7.2
	1.3	Deciduous needleleaf forest	14	5.20	29.1 %	38.3	33.3	199.2	24.5
	2.1	Shrub tundra	50	3.97	22.3 %	49.2	50.8	195.6	24.1
	2.2	Graminoid / forb tundra	114	2.85	15.9 %	72.2	67.5	205.4	25.3
	3.1	Permafrost wetlands	49	0.25	1.4 %	112.2	121.5	28.4	3.5
	3.2	Non-permafrost wetlands	7	0.76	4.3 %	74.5	70.5	56.6	7.0
	5.1	Barren	9	0.85	4.8 %	11.7	14.9	10.0	1.2
	7.1	Yedoma tundra	5	0.27	1.5 %	64.1	37.7	17.5	2.2
	7.2	Yedoma forest	1	0.30	1.7 %	43.0	0.0	13.0	1.6

[a] The number of sampled pedons reaching a full depth of 100 cm or 300 cm, respectively.

[b] Mean SOC storage and SD calculations includes pedons which are not reaching the full section depth.

306

307
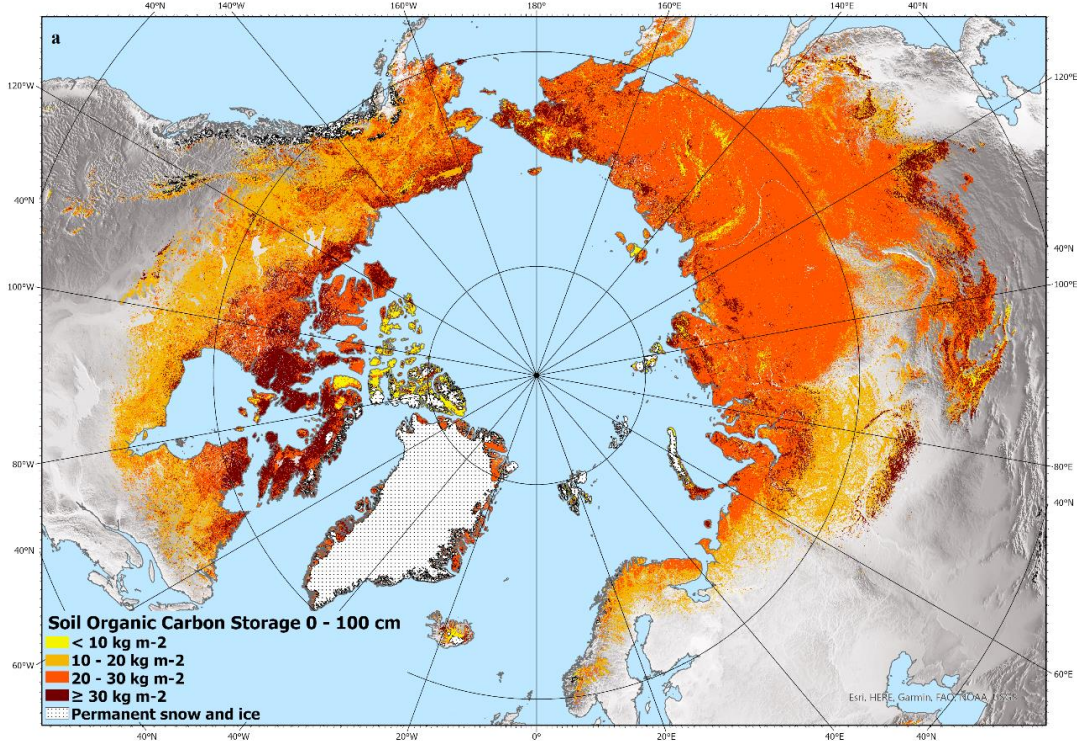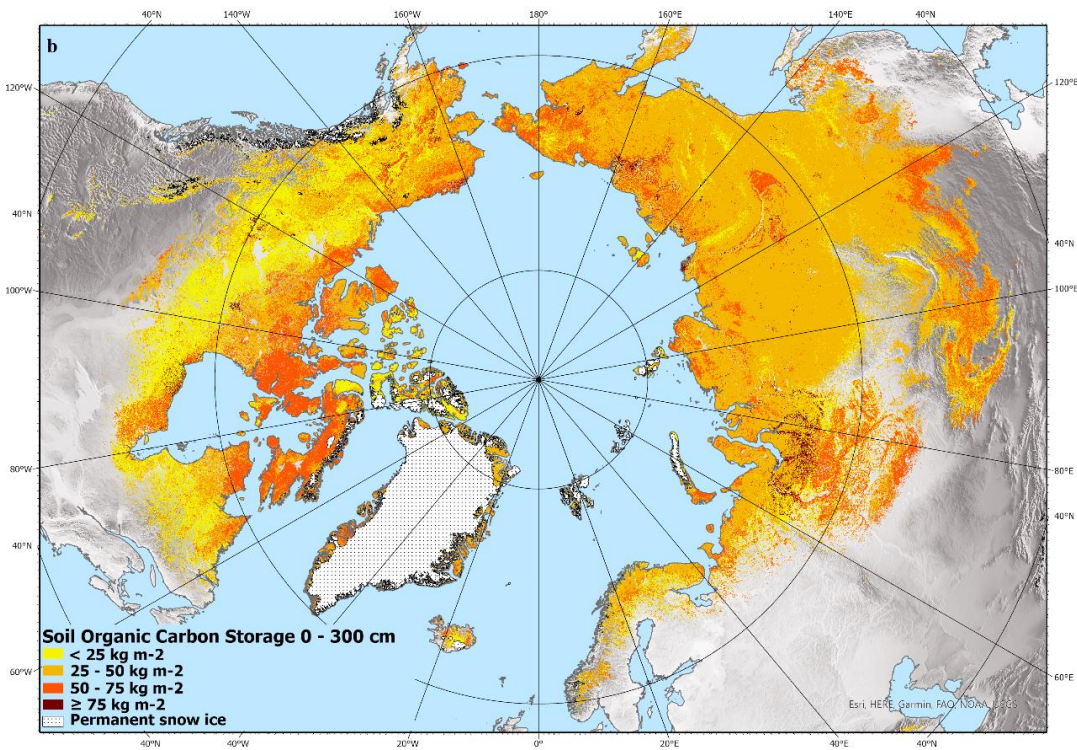
Figure 3. Estimated total SOC storage (kg C m^{-2}) to a depth of 0–100 cm (a) and 0–300 cm (b) in northern circumpolar

permafrost region. North Pole Lambert azimuthal equal area projection (datum: WGS 84). Base map: Made with

Natural Earth.

3.2 TN estimates

Our estimates show that the TN stocks down to 100 cm and 300 cm depth in the northern circumpolar permafrost region are 21.1 Pg and 55.0 Pg, respectively. Table 6 presents the mean and total TN storage for different depth increments with their 95% confidence interval. As with SOC storage, the most abundant land cover classes (deciduous needleleaf forest, shrub tundra and graminoid / forb tundra) store most (68 %) of the total TN in the permafrost region. The land cover classes permafrost and non-permafrost wetlands have the largest TN storage with a mean of up to 7 kg N m^{-2} for the 0–300 cm soil depth (Table 7). Figure 4 illustrates the spatial distribution of total TN storage (kg N m^{-2}) for the circumpolar permafrost region for two depth intervals, 0–100 cm and 0–300 cm. The spatial distribution of TN has a similar pattern to SOC and is highlighting the permafrost peatlands in Western Siberia, Russia and the Nunavut territory in Canada.

Table 6: Mean and total TN storage with 95 % CI for the different depth increments for the northern circumpolar permafrost region, excluding water bodies and permanent snow and ice.

Depth increment		~~Landscape mean~~ Mean TN storage (kg N m^{-2})		95 % CI [a]	Total TN in Pg	95 % CI [a]
0–30 cm	271	0.5	±	0.1	8.1	± 1.5
30–50 cm	250	0.2	±	0.0	4.2	± 0.5
50–100 cm	208	0.5	±	0.1	8.8	± 1.1
100–200 cm	175	1.0	±	0.2	17.1	± 2.8
200–300 cm	169	0.9	±	0.2	16.8	± 3.7
0–100 cm	208	1.2	±	0.3	21.1	± 4.7
0–300 cm	169	3.1	±	0.8	55.0	± 15.1

[a] The 95 % confidence interval refers to landscape mean TN storage and total TN storage

325 Table 7: Mean and total TN storage for (A) 0–100 cm and (B) 0–300 cm soil depth separated for the different Tier
326 classes within the northern circumpolar permafrost region, excluding water bodies and permanent snow and ice.

A	Tier class	LCC class	n [a]:	Area (million km²)	Area %	Mean TN storage (kg N m⁻²) [b]	SD [b]	Total TN in Pg	Total TN storage %
	1.1	Deciduous broadleaf forest	2	0.85	4.8 %	1.0	0.6	0.9	4.1
	1.2	Evergreen needleleaf forest	1	2.54	14.3 %	0.8	0.8	1.9	9.2
	1.3	Deciduous needleleaf forest	19	5.20	29.1 %	1.0	0.6	5.1	24.3
	2.1	Shrub tundra	32	3.97	22.3 %	1.6	1.5	6.4	30.3
	2.2	Graminoid / forbtundra	72	2.85	15.9 %	1.5	0.9	4.3	20.3
	3.1	Permafrost wetlands	46	0.25	1.4 %	2.4	2.5	0.6	2.8
	3.2	Non-permafrost wetlands	4	0.76	4.3 %	0.7	0.6	0.5	2.4
	5.1	Barren	26	0.85	4.8 %	0.7	0.9	0.6	2.6
	7.1	Yedoma tundra	5	0.27	1.5 %	1.6	0.6	0.4	2.0
	7.2	Yedoma forest	1	0.30	1.7 %	1.4	0.0	0.4	2.0

B	Tier class	LCC class	n [a]:	Area (million km²)	Area %	Mean TN storage (kg N m⁻²) [b]	SD [b]	Total TN in Pg	Total TN storage %
	1.1	Deciduous broadleaf forest	2	0.85	4.8 %	2.8	1.7	2.4	4.3
	1.2	Evergreen needleleaf forest	1	2.54	14.3 %	1.9	2.3	4.8	8.8
	1.3	Deciduous needleleaf forest	12	5.20	29.1 %	2.4	1.3	12.6	23.0
	2.1	Shrub tundra	30	3.97	22.3 %	3.9	3.4	15.5	28.2
	2.2	Graminoid / forbtundra	69	2.85	15.9 %	3.4	2.2	9.6	17.5
	3.1	Permafrost wetlands	40	0.25	1.4 %	7.0	7.8	1.8	3.2
	3.2	Non-permafrost wetlands	2	0.76	4.3 %	6.4	6.6	4.9	8.9
	5.1	Barren	9	0.85	4.8 %	0.8	1.1	0.7	1.2
	7.1	Yedoma tundra	3	0.27	1.5 %	5.6	2.2	1.5	2.8
	7.2	Yedoma forest	1	0.30	1.7 %	4.1	0.0	1.2	2.2

327

328 [a] The number of sampled pedons reaching a full depth of 100 cm or 300 cm, respectively.
329 [b] Mean TN storage and SD calculations includes pedons which are not reaching the full section depth.

330
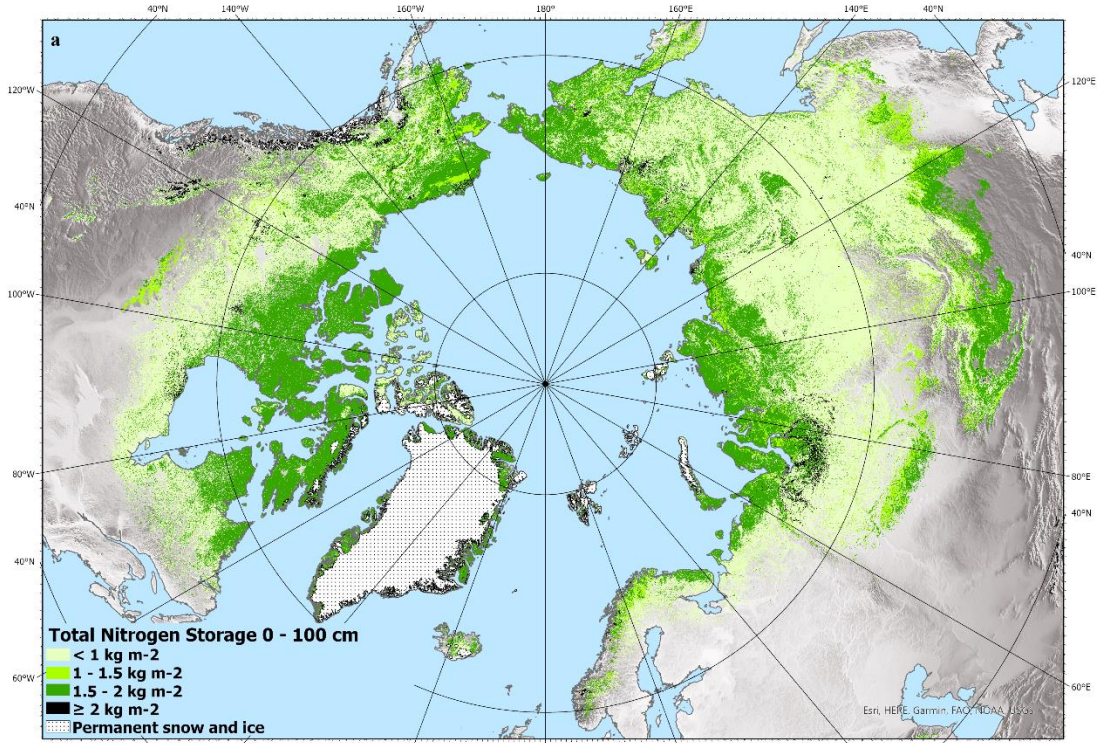
331
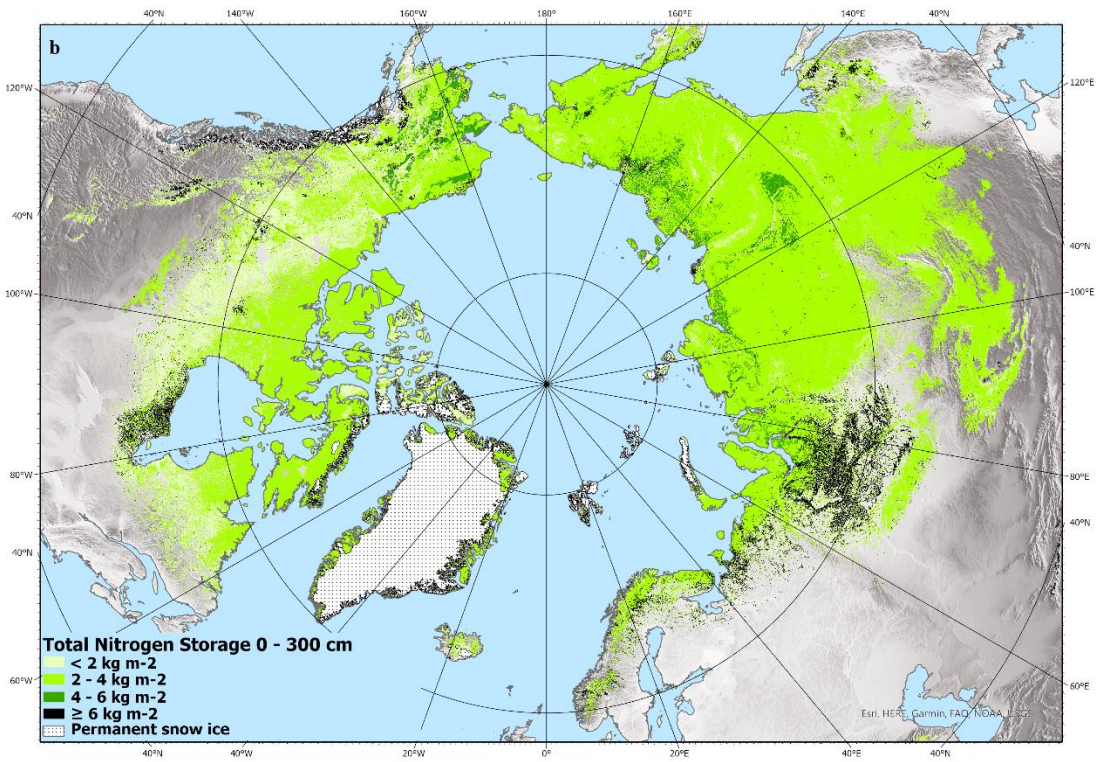
332

333   Figure 4. Estimated total Nitrogen storage (kg N m^{-2}) to a depth of 0–100 cm and 0–300 cm in northern circumpolar

334   permafrost region. North Pole Lambert azimuthal equal area projection (datum: WGS 84). Base map: Made with

335   Natural Earth.

3.3 C/N ratio and δ13C

Carbon to nitrogen ratios are often used as an indicator for SOM decomposition. As during the metabolic activity by microorganisms more carbon than nitrogen is released, the C/N ratio decreases with a higher degree of humification. This is why C/N ratios usually decrease with depth, as deeper layers are typically older and more decomposed (Kuhry and Vitt, 1996). Our data confirms this pattern of fast decreasing C/N ratio with depth in all land cover classes to about 50 cm of depth followed by weak decline throughout the full pedon depth (Figure5 a). The C/N values of SOC rich top soil organic and peat samples are significantly higher than from the mineral samples ($p < 0.05$). The C/N ratios together with stable carbon isotopes (δ^{13}C) can be used to gain insight into the biochemical processes of SOM, botanical origin with depth and the degradation state (Kracht and Gleixner, 2000). The lowest δ13C values, predominantly in the upper 50 cm, indicates that this SOM is more easily available for microbial utilization with lowest values in peatlands connected to differences in hydrology.

3.3 4 Soil stratigraphies

Figure 5 illustrates averaged vertical soil stratigraphies for SOC and TN density, C/N ratio with δ^{13}C, dry bulk density, volumetric fractions for water/ice, organic, mineral, air and texture (sand, silt + clay fraction) separated by land cover class to 300 cm depth. The data shows clear differences occurring in the more variable top meter in comparison to the rather stable second and third meter with the. With an exception in Nonnon-Permafrost permafrost wetlands where the TN and SOC density is more variable below 100 cm depth, which results from only 2 stratigraphy different available pedons where TN data is available (Table 7). Instead, tThe Permafrost permafrost wetland class shows the highest and rather stable consistent stratigraphy for SOC and TN density, which is due to the high organic fraction of these soilsalso supported by the high organic fraction with low DBD and low mineral fraction. In comparison, the barren has the lowest SOC and TN, as these soils are dominated by the coarse mineral fraction Which is the opposite for the Barren class with low SOC and TN surrounded by mainly coarse mineral fraction and from ca. 140 cm depth where alsoeven our deepest barren samples reached bedrock. While the stratigraphy for the Yedoma classes proves the Yedoma typical ice-rich silt sediments visible in the high silt + clay and high water/ice fraction. These important trends are more evident, e.g. high variability in water fraction between classes or high silt + clay fraction, in Yedoma tundra. Stratigraphy for DBD shows a strong dependence with the mineral fraction and almost identical soil stratigraphy.

364

365

366
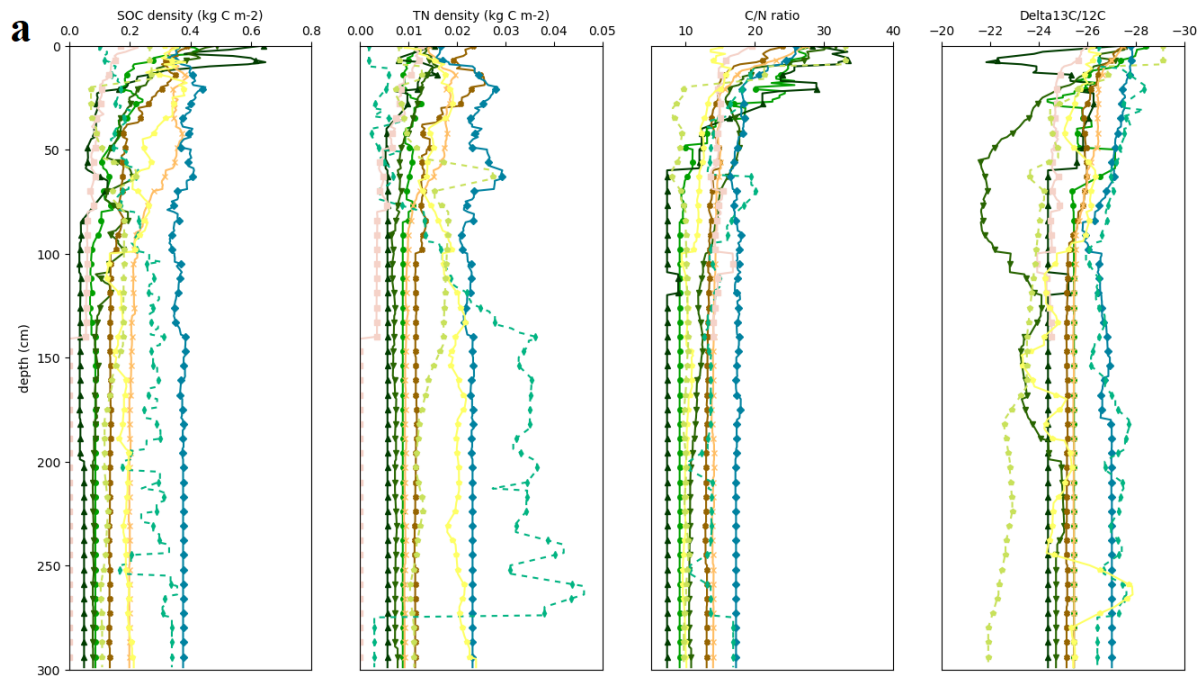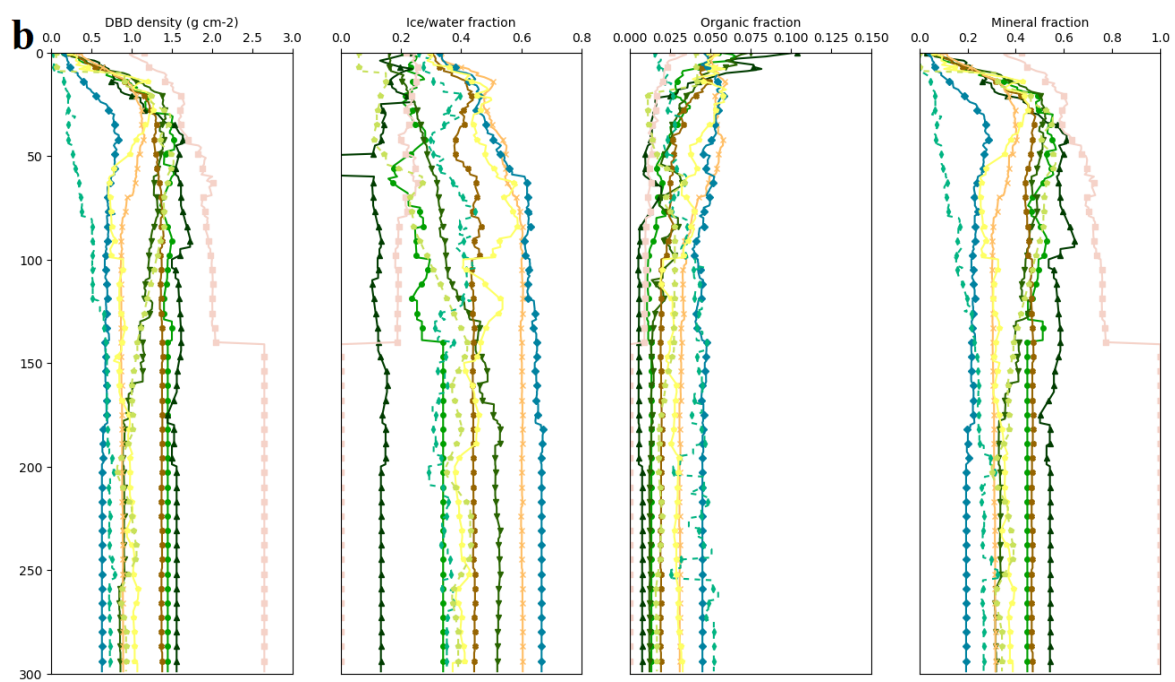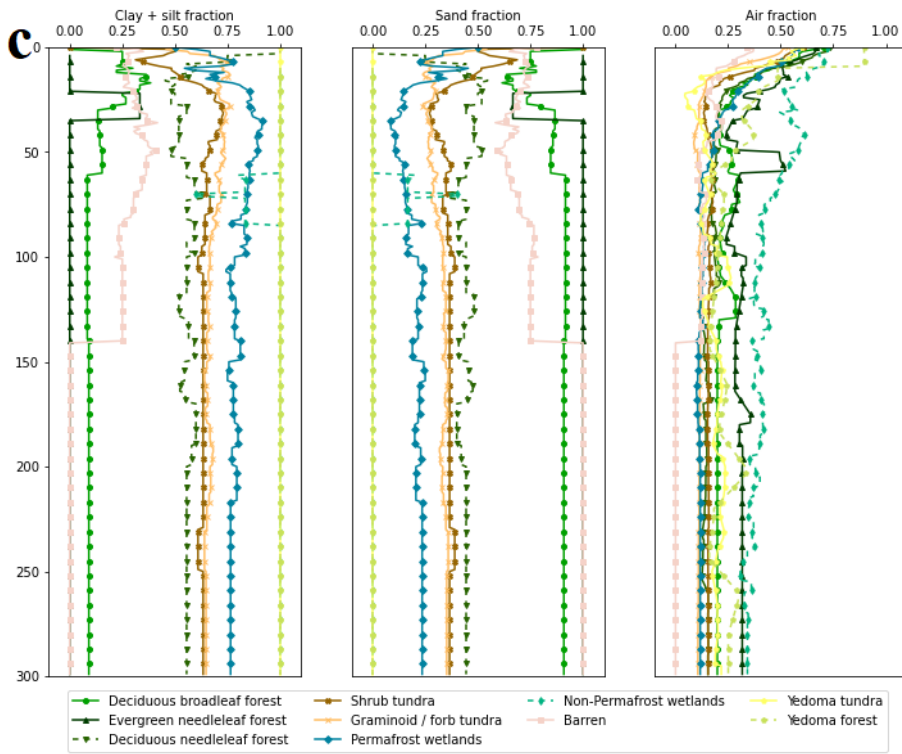
368 Figure 5. Typical vertical soil stratigraphies for all the land cover classes to 300 cm depth separated for SOC density,

369 TN density, C/N ratio and Delta 13C/12C (a); DBD density, Ice/water fraction, Organic fraction and Mineral fraction

370 (b); Clay + silt fraction, Sand fraction and Air fraction (c).

4. Discussion

The goal of the field studies to collect this dataset has mainly been to improve the knowledge base for studies of climate feedbacks resulting from permafrost thaw. This new open access database provides georeferenced and quality assessed soil profile data to serve different scientific communities. While there are multiple databases available containing data on soil carbon storage (Hugelius et al., 2013, Michaelson et al., 2013, Mishra et al., 2021), there is still a lack of soil field data covering a wider range of properties within the hard-accessible northern circumpolar permafrost region.

To test and exemplify usage of the soil profile database, we used our field-based metadata to classify soil profiles according to a coherent land cover scheme and combined it with ESA's land cover product to provide a new estimate of soil organic carbon storage in the northern circumpolar permafrost region. Our estimate for SOC is 380 Pg $\pm$ 58 Pg to 100 cm soil depth and 813 Pg $\pm$ 136 Pg to 300 cm soil depth for the permafrost region occupying an area of 17.9×10^6 km^2 (excluding area of Tibetan permafrost region, permanent snow and ice and water bodies). In comparison, Hugelius et al., (2014) estimated SOC stocks in the northern circumpolar permafrost region (17.8×10^6 km^2 excluding exposed bedrock, glaciers and ice-sheets and water bodies) to be 472 ± 27 Pg and 1035 ± 150 Pg to 100 cm and 300 cm for soils, respectively. A recent publication by Mishra et al., (2021) based on > 2700 soil profiles

386   with environmental variables in a geostatistical mapping framework, estimated a total SOC stock of 510 Pg (– 78 to

387   +79 Pg) and 1000 (– 170 to +186 Pg) to 100 cm and 300 cm, respectively. Although our values are a bit lower than

388   their estimates, they are within each other ~~errors~~ranges. Usage of a different landcover based upscaling approach could

389   be the cause of some of these differences.

390   Despite the importance of nitrogen for microbial decomposition and plant productivity processes, few large-scale

391   datasets are available on TN storage. Our TN estimate for the northern circumpolar permafrost region is 21 Pg ± 5 Pg

392   to 100 cm soil depth and 55 Pg ± 15 Pg to 300 cm soil depth. This is in line with the only other circumpolar estimate

393   of 66 Pg (± 35 Pg) by Harden et al. (2012).

394   According to Kuhry and Vitt (1996), C/N ratios of peat deposits decrease over time due to cumulative anaerobic

395   degradation while in aerobic environment decomposition and release of CO_2 is lowering the C/N ratios in organic and

396   mineral soil horizons (Ping et al., 1998). Our data show that the C/N ratios in organic soil horizons and peat layers

397   were significantly higher than from mineral subsoil horizons. Based on this, we can use the C/N ratio data to assess

398   the relative degree of SOM decomposition on circumpolar scale. However, C/N ratios and stable carbon isotopes are

399   affected by the original plant type and climate.

400   A key element to this upscaling exercise is the accuracy of the land cover dataset. Despite the relatively high spatial

401   resolution of 300 m, many Arctic landscape features cannot be represented at this scale. Although, ESA's land cover

402   map has a good overall accuracy of 73 %; however, this means that 27 % of the land cover is possibly mismatched

403   and in need of improvement. Moreover, the accuracy for natural and semi-natural aquatic vegetation, which

404   corresponds to our wetland class, is unfortunately as low as 19 % which corresponds to our class (wetland). According

405   to Hugelius et al. (2020), the areal extent of peatlands for the northern permafrost region (3.7×10^6 km^2) is almost

406   four times the ESA's land cover product estimated areal extent (1.0×10^6 km^2). Therefore, wrongly classified areas

407   would partly explain our lower estimate for SOC and TN on a circumpolar scale since the wetland classes have the

408   largest SOC and TN contents, particularly at greater depths (100–300 cm). ~~Which is also visibl~~This is evident ~~e~~ on

409   maps (Figure 3 and Figure 4) where areas classified as peatlands are clearly standing out with their high SOC and TN

410   contents. If we exchange the ESA wetland areal coverage for the values from Hugelius et al. (2020) to 3.7×10^6 km^2

411   (2.0×10^6 km^2 in permafrost-free peatlands and 1.7×10^6 km^2 permafrost-affected peatlands) and deduct this in

412   proportion from the other classes, our updated SOC and TN stock to 300 cm soil depth increases from 813 Pg ± 136

413   Pg to 954 Pg ± 162 Pg and from 55 Pg ± 15 Pg to 66 Pg ± 22 Pg, respectively.

414   Even though the current estimates are based on 651 soil pedons from 16 different study areas, there are uncertainties

415   and data gaps for several regions and ecosystems. With e.g. only one high alpine site and one Yedoma forest site,

416   several areas are highly underrepresented. Also, the study areas are concentrated in European and Russian locations

417   which additionally increases the uncertainties in current estimates. Therefore, combining this data with other datasets

418   especially from North America, Tibet, Yedoma sites and a different wetland extent would substantially reduce

419   potential error sources and create a more complete picture of SOC and TN storage estimates from land cover based

420   upscaling. To our knowledge, this is the first product which presents a more complete dataset in regard to variables

421   on a circumpolar scale that are commonly used to parameterize earth system models. With this database we aim to

422   provide georeferenced point data that can easily be implemented and used for geospatial analysis at a circumpolar

423   scale. This upscaling approach was chosen because this database can be easily extended with additional sampling

424   sites, higher-resolution land cover maps that will further increase the resolution on a circumpolar scale. This data can

425   also be used for upscaling in a particular area of interest. This will assist to quantify and model ongoing pedological

426   and ecological processes relevant to climate change. Furthermore, this may help identifying regions that are more

427   vulnerable to permafrost degradation and greenhouse gas release due to knowledge on texture, water/ice content or

428   SOC storage.

5. Conclusion

430   This dataset represents a substantial contribution of high-quality soil pedon data and metadata across the northern

431   permafrost region. Our land cover based estimates of total SOC to 100 cm and 300 cm soil depth are 380 Pg ± 58 Pg

432   and 813 Pg ± 136 Pg, respectively. In addition, we contribute with novel TN estimates for the different land cover

433   classes and depth increments. Our TN estimate to 100 cm and 300 cm soil depth are 21.1 ± 4.7 Pg and 55 Pg ± 15 Pg

434   which is in line with the only other product available on that scale for TN. Despite a different methodology, are similar

435   but on the lower edge to other recent numbers. We provide data for a wide range of environments and geographical

436   regions across the permafrost region including georeferencing and metadata. This serves as a base that can be easily

437   combined and extended with data from other sources, as several regions are underrepresented (Alaska, Canada, Tibet).

438   This dataset offers high scientific value as it also contains data on chemical and physical soil properties across the

439   northern circumpolar permafrost region. This additional data can be used to develop or parametrize broad scale models

440   and to help better understand different aspects of the permafrost-carbon climate feedback.

6. Data access

442   Two separated datasets are freely available on the Bolin Centre data set repository (https://bolin.su.se/data/). The

443   dataset (Detailed pedon data on soil carbon and nitrogen for the northern permafrost region,

444   https://doi.org/10.17043/palmtag-2022-pedon-1) (Palmtag et al., 2022a) is a geospatial dataset of physical and

445   chemical soil properties from 651 soil pedons and the second dataset (A high spatial resolution soil carbon and nitrogen

446   dataset for the northern permafrost region, https://doi.org/10.17043/palmtag-2022-spatial-1) (Palmtag et al., 2022b)

447   contains GIS grids of the northern circumpolar permafrost region for SOC, TN and C/N ratios for the different depth

448   increments.

449

Funding

This study was funded through the European Space Agency CCI + Permafrost project (4000123681/18/I-NB), the European Union Horizon 2020 research and innovation project Nunataryuk (773421), the Changing Arctic Ocean (CAO) program project CACOON (NE/R012806/1) and the Swedish Research Council (2018-04516).

Author contribution

GH, PK, SW and JP designed the concept of the study. JO wrote the script in Python. JP wrote the initial draft of the manuscript. All authors contributed to the writing and editing of the manuscript.

Competing Interests

The authors declare that they have no conflict of interest.

Acknowledgements

We thank the ESA CCI Land Cover project for providing the data, which was used for upscaling our product to circumpolar scale.

References

Batjes, N.H.: Harmonized soil property values for broad-scale modelling (WISE30sec) with estimates of global soil carbon stocks, *Geoderma*, Vol. 269, https://doi.org/10.1016/j.geoderma.2016.01.034, 2016.

Biskaborn, B. K., Smith, S. L., Noetzli, J., Matthes, H., Vieira, G., Streletskiy, D. A., Schoeneich, P., Romanovsky, V. E., Lewkowicz, A. G., Abramov, A., Allard, M., Boike, J., Cable, W. L., Christiansen, H. H., Delaloye, R., Diekmann, B., Drozdov, D., Etzelmüller, B., Grosse, G., Guglielmin, M., Thomas Ingeman-Nielsen, T., Ketil Isaksen, K., Ishikawa, M., Johansson, M., Johannsson, H., Joo, A., Kaverin, D., Kholodov, A., Konstantinov, P., Kröger, T., Lambiel, C., Lanckman, J.-P., Luo, D., Malkova, G., Meiklejohn, I., Moskalenko, N., Oliva, M., Phillips, M., Ramos, M., Sannel, A. B. K., Sergeev, D., Seybold, C., Skryabin, P., Vasiliev, A., Wu, Q., Yoshikawa, K., Zheleznyak, M. and Lantuit, H.: Permafrost is warming at a global scale, *Nature Communications*, 10(1), 264, https://doi.org/10.1038/s41467-018-08240-4, 2019.

Czekirda, J., Westermann, S., Etzelmüller, B. and Johanneson, T.: Transient modelling of permafrost distribution in Iceland. *Frontiers in Earth Science*, 7, 130, https://doi.org/10.3389/feart.2019.00130, 2019.

476 Defourny, P., Schouten, L., Bartalev, S.A., Bontemps, S., Caccetta, P., de Wit, A.J.W., Di Bella, C., Gerard, B., Giri,

477 C., Gong, V., Hazeu, G.W., Heinimann, A., Herold, M., Knoops, J., Jaffrain, G., Latifovic, R., Lin, H., Mayaux, P.,

478 Måcher, C.A., Nonguierma, A., Stibig, H.J., Van Bogaert, E., Vancutsem, C., Bicheron, P., Leroy, M. and Arino, O.:

479 Accuracy assessment of a 300 m global land cover map: The GlobCover experience. Available online: http://www.un-

480 spider.org/space-application/space-application-matrix/accuracy-assessment-300-m-global-land-cover-map-

481 globcover (accessed on 07 January 2022), 2008.

482 ESA Climate Change Initiative-Landcover visualization interface, Available from:

483 http://maps.elie.ucl.ac.be/CCI/viewer/index.php (accessed on 07 January 2022), 2017.

484 Farouki, O. T.: Thermal Properties of Soils, Cold regions research and engineering lab Hanover NH [online] Available

485 from: https://apps.dtic.mil/docs/citations/ADA111734 (accessed on 07 January 2022), 1981.

486 Flato, G. M.: Earth system models: an overview, 2, 783–800, https://doi.org/10.1002/wcc.148, 2011.

487 Fritz, M., Vonk, J.E. and Lantuit, H.: Collapsing Arctic coastlines, *Nature Climate Change*, volume 7,

488 https://doi.org/10.1038/nclimate3188, 2017.

489 Fuchs, M., Kuhry, P., and Hugelius, G.: Low below-ground organic carbon storage in a subarctic Alpine permafrost

490 environment, *The Cryosphere*, 9, 427–438, https://doi.org/10.5194/tc-9-427-2015, 2015.

491 Global Soil Data Task: Global soil data products CD-ROM contents (IGBP-DIS), ORNL DAAC, 2014.

492 Gruber, S.: Derivation and analysis of a high-resolution estimate of global permafrost zonation, *The Cryosphere*, 6,

493 221–233, https://doi.org/10.5194/tc-6-221-2012, 2012.

494 Harden, J.W., Koven, C.D., Ping, C.-L., Hugelius, G., McGuire, A.D., Camill, P., Jorgenson, T., Kuhry, P.,

495 Michaelson, G.J., O'Donnell, J.A., Schuur, E.A.G., Tarnocai, C., Johnson, K. and Grosse, G.: Field information links

496 permafrost carbon to physical vulnerabilities of thawing. *Geophysical Research Letter*, 39, L15704,

497 https://doi.org/10.1029/2012GL051958, 2012.

498 Heiri, O., Lotter, A. F., and Lemcke, G.: Loss on ignition as a method for estimating organic carbon and carbonate

499 content in sediments: reproduction and comparability of results. *J. Paleolimnol.*,25,101–110,

500 https://doi.org/10.1023/a:1008119611481, 2001.

501 Hugelius G. and Kuhry, P.: Landscape partitioning and environmental gradient analyses of soil organic carbon in a

502 permafrost environment. *Global Biogeochem. Cycles*, 23, GB3006, https://doi.org/10.1029/2008GB003419, 2009.

503 Hugelius G., Kuhry, P., Tarnocai, C. and Virtanen, T.: Soil organic carbon pools in a periglacial landscape: a case

504 study from the central Canadian Arctic. *Permafrost Periglac. Process.*, 21: 16-29. https://doi.org/10.1002/ppp.677,

505 2010.

506 Hugelius, G., Virtanen, T., Kaverin, D., Pastukhov, A., Rivkin, F., Marchenko, S., Romanovsky, V. and Kuhry, P.:

507 High-resolution mapping of ecosystem carbon storage and potential effects of permafrost thaw in periglacial terrain,

508 European Russian *Arctic, J. Geophys. Res.*, 116, G03024, https://doi.org/10.1029/2010JG001606, 2011.

509 Hugelius, G.: Spatial upscaling using thematic maps: An analysis of uncertainties in permafrost soil carbon estimates.
510 *Global Biogeochem Cycles* GB2026. https://doi.org/10.1029/2011GB004154, 2012.

511 Hugelius, G., Bockheim, J. G., Camill, P., Elberling, B., Grosse, G., Harden, J. W., Johnson, K., Jorgenson, T., Koven,
512 C. D., Kuhry, P., Michaelson, G., Mishra, U., Palmtag, J., Ping, C.-L., O'Donnell, J., Schirrmeister, L., Schuur, E. A.
513 G., Sheng, Y., Smith, L. C., Strauss, J., and Yu, Z: A new data set for estimating organic carbon storage to 3 m depth
514 in soils of the northern circumpolar permafrost region. *Earth Syst. Sci. Data*, 5, 393–402, https://doi.org/10.5194/essd-
515 5-393-2013, 2013.

516 Hugelius, G., Strauss, J., Zubrzycki, S., Harden, J. W., Schuur, E. A. G., Ping, C.-L., Schirrmeister, L., Grosse, G.,
517 Michaelson, G. J., Koven, C. D., O'Donnell, J. A., Elberling, B., Mishra, U., Camill, P., Yu, Z., Palmtag, J., and Kuhry,
518 P.: Estimated stocks of circumpolar permafrost carbon with quantified uncertainty ranges and identified data gaps.
519 *Biogeosciences* 11(23):6573– 6593, https://doi.org/10.5194/bg-11-6573-2014, 2014.

520 Hugelius, G., Loisel, J., Chadburn, S., Jackson, R.B., Jones, M., MacDonald, G., Marushchak, M., Olefeldt, D.,
521 Packalen, M., Siewert, M.B., Treat, C., Turetsky, M., Voigt, C. and Yu, Z.: Large stocks of peatland carbon and
522 nitrogen are vulnerable to permafrost thaw. *PNAS*, 117, 34, https://doi.org/10.1073/pnas.1916387117, 2020.

523 Köchy, M., Hiederer, R., and Freibauer, A.: Global distribution of soil organic carbon – Part 1: Masses and frequency
524 distributions of SOC stocks for the tropics, permafrost regions, wetlands, and the world, *SOIL*, 1, 351–365,
525 https://doi.org/10.5194/soil-1-351-2015, 2015.

526 Kracht, O and Gleixner, G.: Isotope analysis of pyrolysis products from Sphagnum peat and dissolved organic matter
527 from bog water. Organic *Geochemistry* , 31: 645–654, https://doi.org/10.1016/S0146-6380(00)00041-3, 2020.

528 Kuhry, P. and Vitt, D.H.: Fossil Carbon/Nitrogen Ratios as a Measure of Peat Decomposition. *Ecology*, 77: 271-275.
529 https://doi.org/10.2307/2265676, 1996.

530 Kuhry, P., Mazhitova, G.G., Forest, P.-A., Deneva, S.V., Virtanen, T. and Kultti, S.: Upscaling soil organic carbon
531 estimates for the Usa Basin (Northeast European Russia) using GIS-based land cover and soil classification schemes.
532 *Geografisk Tidsskrift-Danish Journal of Geography*, 102:1, 11-25, https://doi.org/10.1080/00167223.2002.10649462,
533 2002.

534 McKinney, W.: "pandas: a foundational Python library for data analysis and statistics." Python for high performance
535 and scientific computing 14.9, 1-9, 2011.

536 Michaelson, G.J., Ping, C.-L. and Clark, M.: Soil Pedon Carbon and Nitrogen Data for Alaska: An Analysis and
537 Update. *Open Journal of Soil Science*, 2013, 3, 132-142 http://dx.doi.org/10.4236/ojss.2013.32015, 2013.

538 Mishra, U., Hugelius, G., Shelef, E., Yang, Y., Strauss, J., Lupachev, A., Harden, J.W., Jastrow, J.D., Ping, C.-L.,
539 Riley, W.J., Schuur, E.A.G., Matamala, R., Siewert, M., Nave, L.E., Koven, C.D., Fuchs, M., Palmtag, J., Kuhry, P.,
540 Treat, C.C., Zubrzycki, S., Hoffman, F.M., Elberling, B., Camill, P., Veremeeva, A. and Orr, A.: Spatial heterogeneity
541 and environmental predictors of permafrost region soil organic carbon stocks. *Science Advances*, 7, 9, https://doi.org/
542 10.1126/sciadv.aaz5236, 2021.

Nachtergaele, F., van Velthuizen, H., Verelst, L., Batjes, N.H., Dijkshoorn, K., van Engelen, V.W.P., Fischer, G., Jones, A. and Montanarela, L.: The harmonized world soil database, in Proceedings of the 19th World Congress of Soil Science, Soil Solutions for a Changing World, Brisbane, Australia, 1-6 August 2010, pp. 34–37, 2010.

National Wetlands Working Group. The Canadian Wetland Classification System, 2nd Edition. Warner, B.G. and C.D.A. Rubec (eds.), Wetlands Research Centre, University of Waterloo, Waterloo, ON, Canada. 68 p, 1997.

Obu, J., Westermann, S., Bartsch, A., Berdnikov, N., Christiansen, H.H., Dashtseren, A., Delaloye, R., Elberling, B., Etzelmuller, B., Kholodov, A., Khomutov, A., Kääb, A., Leibman, M.O., Lewkowicz, A.G., Panda, S.K., Romanovsky, V., Way, R.G., Westergaard-Nielsen, A., Wu, T., Yamkhin, J. and Zou, D.: Northern Hemisphere permafrost map based on TTOP modelling for 2000–2016 at 1 km2 scale, *Earth-Science Reviews* 193, https://doi.org/10.1016/j.earscirev.2019.04.023, 2019.

Obu, J.: How much of the Earth's surface is underlain by permafrost? *Journal of Geophysical Research: Earth Surface*, 126, e2021JF006123. https://doi.org/10.1029/2021JF006123, 2021

Oleson, K. W., Lawrence, D. M., Bonan, G.B., Flanner, M.G., Kluzek, E., Lawrence, P.J., Levis, S., Swenson, S.C., Thornton, P.E., Dai, A., Decker, M., Dickinson, R., Feddema, J., Heald, C.L., Hoffman, F., Lamarque, J.-F., Mahowald, N., Niu, G.-Y., Qian, T., Randerson, J., Running, S., Sakaguchi, K., Slater, A., Stockli, R., Wang, A., Yang, Z.-L., Zeng, X., and Zeng, X.: Technical description of version 4.0 of the Community Land Model (CLM), 2010.

Palmtag, J., Hugelius, G., Lashchinskiy, N., Tarmstorf, M.P., Richter, A., Elberling, B. and Kuhry, P.: Storage, landscape distribution and burial history of soil organic matter in contrasting areas of continuous permafrost, *Arct. Antarct. Alp. Res.*, 47, 71–88, https://doi.org/10.1657/AAAR0014-027, 2015.

Palmtag, J., Ramage, J., Hugelius, G., Gentsch, N., Lashchinskiy, N., Richter, A. and Kuhry, P.: Controls on the storage of organic carbon in permafrost soils in northern Siberia, *Eur. J. Soil Sci.*,67, 478–491, https://doi.org/10.1111/ejss.12357, 2016.

Palmtag, J. and Kuhry, P.: Grain size controls on cryoturbation and soil organic carbon density in permafrost-affected soils. *Permafrost and Periglac Process*, 29, https://doi.org/10.1002/ppp.1975, 2018.

Palmtag, J., Obu, J., Kuhry, P., Siewert, M., Weiss, N. and Hugelius, G.: Detailed pedon data on soil carbon and nitrogen for the northern permafrost region. Dataset version 1. Bolin Centre Database. https://doi.org/10.17043/palmtag-2022-pedon-1, 2022a.

Palmtag, J., Obu, J., Kuhry, P., Siewert, M., Weiss, N. and Hugelius, G.: A high spatial resolution soil carbon and nitrogen dataset for the northern permafrost region. Dataset version 1. Bolin Centre Database. https://doi.org/10.17043/palmtag-2022-spatial-1, 2022b.

Pascual, D., Kuhry, P. and Raudina, T.: Soil organic carbon storage in a mountain permafrost area of Central Asia (High Altai, Russia). *Ambio*. https://doi.org/10.1007/s13280-020-01433-6, 2020.

576 Ping, C.L., Bockheim, J.G., Kimble, J.M., Michaelson J.J. and Walker, D.A.: Characteristics of cryogenic soils along
577 a latitudinal transect in arctic Alaska. J. Geophys. Res.: Atmos. 103, 917–928, https://doi.org/10.1029/98JD02024,
578 1998.

579 Pribyl, D. W.: A critical review of the conventional SOC to SOM conversion factor, Geoderma, 156(3), 75–83,
580 https://doi.org/10.1016/j.geoderma.2010.02.003, 2010.

581 Siewert, M.B., Hanisch, J., Weiss, N., Kuhry, P., Maximov, T.C. and Hugelius, G.: Comparing carbon storage of
582 Siberian tundra and taiga permafrost ecosystems at very high spatial resolution. *JGR - Biogeosciences*, Volume 120,
583 https://doi.org/10.1002/2015JG002999, 2015.

584 Siewert, M.B., Hugelius, G., Heim, B. and Faucherre, S.: Landscape controls and vertical variability of soil organic
585 carbon storage in permafrost-affected soils of the Lena River Delta. *CATENA*, Volume 147, Pages 725-741,
586 https://doi.org/10.1016/j.catena.2016.07.048, 2016.

587 Siewert, M. B.: High-resolution digital mapping of soil organic carbon in permafrost terrain using machine learning:
588 a case study in a sub-Arctic peatland environment, *Biogeosciences*, 15, 1663–1682, https://doi.org/10.5194/bg-15-
589 1663-2018, 2018.

590 Siewert, M.B., Lantuit, H., Richter, A. and Hugelius, G.: Permafrost Causes Unique Fine-Scale Spatial Variability
591 Across Tundra Soils. *Global Biogeochemical Cycles*, 35, e2020GB006659. https://doi.org/10.1029/2020GB006659,
592 2021.

593 Strauss, J., Schirrmeister, L., Grosse, G., Fortier, D., Hugelius, G., Knoblauch, C., Romanovsky, V., Schädel, C.,
594 Schneider von Deimling, T., Schuur, T.A.G., Shmelev, D., Ulrich, M. and Veremeeva, A.: Deep Yedoma permafrost:
595 A synthesis of depositional characteristics and carbon vulnerability, *Earth-Science Reviews*, Volume 172,
596 https://doi.org/10.1016/j.earscirev.2017.07.007, 2017.

597 Thomson, S.K. Sampling. New York: John Wiley, 343 pp., 1992.

598 Turetsky, M.R., Abbott, B.W., Jones, M.C., Anthony, K.W., Olefeldt, D., Schuur, T.A.G., Koven, C., McGuire, A.D.,
599 Grosse, G., Kuhry, P., Hugelius, G., Lawrence, D.M., Gibson, C. and Sannel, A.B.K.: Permafrost collapse is
600 accelerating carbon release, *Nature*, 569, https://doi.org/10.1038/d41586-019-01313-4, 2019.

601 Weiss, N., Blok, D., Elberling, B., Hugelius, G., Jörgensen, C.J., Siewert, M.B. and Kuhry, P.: Thermokarst dynamics
602 and soil organic matter characteristics controlling initial carbon release from permafrost soils in the Siberian Yedoma
603 region. *Sedimentary Geology*, 340, 38-48, https://doi.org/10.1016/j.sedgeo.2015.12.004, 2016.

604 Weiss, N., Faucherre, S., Lampiris, N. and Wojcik, R.: Elevation-based upscaling of organic carbon stocks in High-
605 Arctic permafrost terrain: a storage and distribution assessment for Spitsbergen, Svalbard. *Polar Research*, 36,
606 https://doi.org/10.1080/17518369.2017.1400363, 2017.

607 Westermann, S., Schuler, T. V., Gisnås, K. and Etzelmüller, B.: Transient thermal modeling of permafrost conditions
608 in Southern Norway, *The Cryosphere*, 7, 719–739, https://doi.org/10.5194/tc-7-719-2013, 2013.

609 Westermann, S., Peter, M., Langer, M., Schwamborn, G., Schirrmeister, L., Etzelmüller, B., and Boike, J.: Transient
610 modeling of the ground thermal conditions using satellite data in the Lena River delta, Siberia, *The Cryosphere*, 11,
611 1441–1463, doi.org/10.5194/tc-11-1441-2017, 2017.

612 Wojcik, R., Palmtag, J., Hugelius, G., Weiss, N. and Kuhry, P.: Landcover and landform-based upscaling of soil
613 organic carbon stocks on the Brøgger Peninsula, Svalbard, *Arctic, Antarctic, and Alpine Research*, 51:1, 40-57,
614 https://doi.org/ 10.1080/15230430.2019.1570784, 2019.